

2- 3 Study on the ionosphere disturbance before large earthquake *

- Report from the Ionosphere Precursor Study Group, 2 -

K. -I. Oyama^{1,2,3}, C. H. Chen⁴, D. Minakshi⁵, L. Bankov⁶, K. Ryu⁷, J. Y. Liu⁸, H. Liu^{1,9}, and T. Uozumi¹,

1 International Center for Space Weather Study and Education, Kyushu University, Fukuoka, Japan

2 Institute of Plasma and Space Science, National Cheng Kung University, Taiwan

3. Coltd Asia Space Environment Research Consortium, Sagamihara, Japan

4 Department of Earth Science, National Cheng Kung University, Tainan, Taiwan

5 Physics department, Gauhati University, Assam, India

6 Space Research and Technology Institute - Bulgarian Academy of Sciences, Sofia, Bulgaria

7 Satellite Technology Research Center, Korea Advanced Institute of Science and Technology, Daejeon, Republic of Korea

8 Institute of Space Science, National Central University, Chung-Li, Taiwan

9 Department of Earth and Planetary Sciences, Kyushu University, Fukuoka, Japan

Abstract: Electric field seems to be a main driver which disturbs ionosphere prior to large earthquake. The problem is where and how the electric field is generated. First part of this paper, we present data observed with US satellite, Dynamic Explorer 2 (DE-2) which is used to discuss our idea on the generation of electric field. We propose here that electric field is originally dynamo field which appears around 100 km. It only enhances around the epicenter region. That is, during daytime the eastward electric field is enhanced, while during night time, westward electric field is enhanced. As a result of enhanced eastward/westward electric field, plasma density over the geomagnetic equator increases both day and night time. During day time, plasma is lifted to higher altitude, causing plasma density increase because of its less recombination with neutral particles. At the same time, magnetic flux tube is filled by the plasma. During night time plasma which is lifted up during daytime is pushed down. This process causes increase of plasma density around F region and topside ionosphere. In high latitude, night time enhancement of F region plasma density is more clearly observed because plasma which is stored in the large magnetic flux tube is continuously supplied. Although the mechanism of the enhanced dynamo field is not so clear, we suggest that internal gravity wave of small amplitude which is generated before large earthquake nonlinearly interacts with planetary scale wave, and is amplified. The internal gravity thus amplified enhances the dynamo electric field and /or neutral density at dynamo region as well as F region.

1. Satellite data analysis

The paper is a continuation of the first paper [Oyama et al, 2016], which reports the outcome from ionosphere precursor study group (IPSG) conducted in 2015-2016. As the first paper does not discuss in detail on the electric field, we concentrate to discuss the electric field which is one of the most probable source to disturb ionosphere before large earthquake by using O⁺ density and Plasma drift measured with US satellite ,DE-2 .

* The manuscript will be submitted to refereed Journal after the major revision

2. DE-2 data, Precursor Ionization Anomaly

Dynamic explorer satellite DE-2 was in orbit during August 13 1981, and February 19 1983. Inclination of the satellite orbit is 89.99° , and perigee and apogee heights are 309-1012 Km respectively. The ionosphere which were measured are electron density N_e , electron temperature T_e , ion composition such as O^+ , M^+ (molecular ions), ion temperature T_i , plasma drift velocity of 3 components, neutral density, wind, and temperature. Basically a royal road to find the special feature associated with large ($M > 6-7$) earthquake is to first construct model by using data observed, and then to find the deviation of ionosphere parameter from the model. The model needs to include local time, latitude longitude, season, and height as basis input parameter at least. No so much effort has been conducted so far to include the effect of geomagnetic disturbance on the ionosphere. If the satellite takes a circular orbit, satellite height does not need to be parameterized. Data obtained by DE-2 satellite was not proper because of the two reasons: the eccentric orbit of the satellite, and scarce data in lower latitude region where earthquake often occurs because main objective of the DE-2 mission was to study high latitude region. Therefore we tried to find the earthquake case for which clear feature related to earthquake is identified at -300km. As a result only two earthquakes were studied deeply. Basic information of the two earthquakes are 16 Oct. 1981, -33.1°N/-73.1°E, $M_s=7.5$, $D=33$ km, and 7 June 1981, 16.6°N, -96.15°E, $M_s=7$, $D=33.8$ km. The information are obtained from USGS website <http://earthquake.usgs.gov/earthquakes/search/>.

Fig.1 shows O^+ density along satellite orbit from 5 days before to earthquake day for the EQ 16 Oct. 1981, -33.1°N/-73.1°E, $M_s=7.5$, $D=33$ km [Oyama et al., 2011]. The DE-2 satellite flew from southern to northern hemisphere. One minimum exists at around geomagnetic equator as black arrow in the 2nd, 3rd and 4th (12th, 13rd, and 14th October) shows. The first minimum corresponds to a trough of Equator Ionization Anomaly (EIA). The second minimum (marked by a red arrow) is seen near the epicenter on the 1st, 2nd, and 3rd (grey color line) panel. The 4th panel (2 days before the earthquake) is special; at high latitude in southern hemisphere O^+ density is lower than compared with those of other panels, which is considered due to the atmosphere heating caused by energetic particles. AU and AL index show intense disturbance 2 days before. On the 15th and 16th, only one minimum appears around the epicenter latitude. In most of the satellite passes two minima are identified. When the epicenter is far from geomagnetic equator, three minima appear. For example satellite pass drawn by black color in the 3rd panel (the 13th Oct) shows the third minimum at the latitude of -27° between two minima at the latitudes of -36° , and -7° respectively as are marked by vertical straight lines.

The mechanism of the 2nd minimum generation is the same as for EIA, because upward plasma drift prevails around the epicenter as we show later by Electric field measurement. That is, plasma is lifted up by the eastward natural electric field, and the lifted plasma flows along the geomagnetic line of force (Fountain effect). We think that the feature which is similar to EIA happens over the epicenter. Because of the similarity with EIA, we named the earthquake related feature as Precursor Ionization Anomaly (PIA).

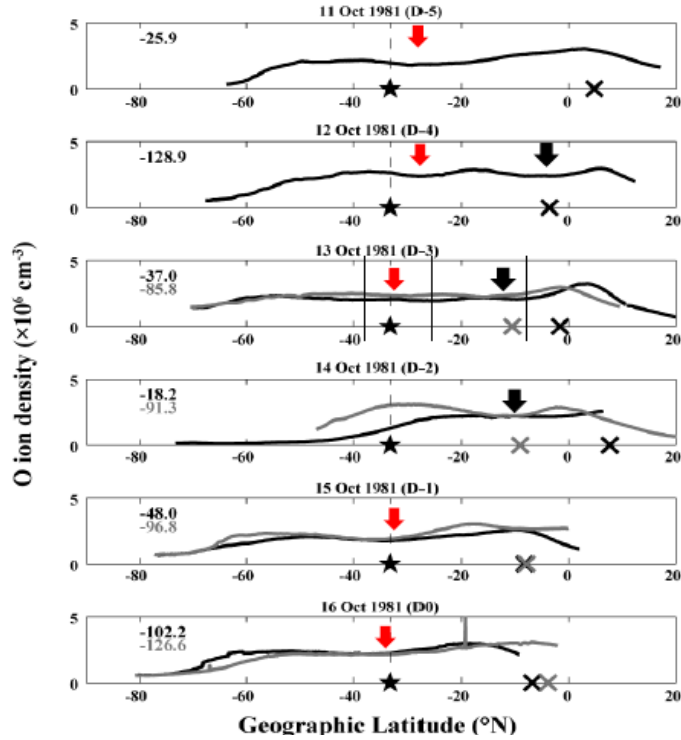


Fig.1 Atomic ion oxygen density along the satellite orbit measured by DE-2 satellite for the earthquake 16 Oct.1981, $-33.1^{\circ}\text{N}/-73.1^{\circ}\text{E}$, $M_s=7.5$, $D=33\text{km}$ [Oyama et al.,2011]. From the top to below, atomic ion density along the satellite orbit is shown for 5 days, 4 days , 3 days , 2 days and 1 days and earthquake day. Cross and star symbols show magnetic equator, and epicenter respectively. Black and grey curves at each panel show the atomic oxygen ion density along different orbit. Red arrow show the minimum which is close to the epicenter, while black arrow shows the minimum near the geomagnetic equator. Three vertical line on 13 Oct.(3rd panel from the top) shows the positions of 3 minima for the orbit of -37.6°N .

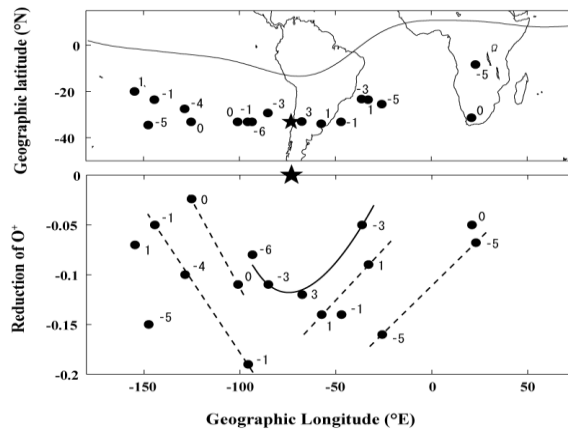


Fig.2 Upper panel :location of two(three) minima of O^+ density[Oyama et al., 2011]. Lower panel shows the reduction of O^+ density versus longitude. A star indicates the epicenter. Number on the right side of the data are days from the earthquake day. Number which has minus sign shows before earthquake. Data which were measured on the same day are connected by dashed line. Black line which connects the

data on 6 and 3 days before and 3 days after is drawn to show a general feature: the maximum reduction of O⁺ occurs around the epicenter.

Fig.2 shows the location of the epicenter and the day of earthquake. In the upper panel two minima merges at one place, that is, the epicenter. The lower panel indicates the ratio of O⁺ density at the minimum to O⁺ of ambient plasma with regard to longitude.

The maximum reduction of O⁺ is about 20 %. These two figures shows that by plotting the location of minimum, and the reduction of O⁺ density, the location of the epicenter can be identified. It is noted that O⁺ density does not reduce continuously toward earthquake day: one day it is high, and another day it is low. The minimum of molecular ions, most probably NO⁺ ion shows the similar feature.

Fig.3 shows the location shifting of the two (three) minima versus days from the earthquake day. The first minimum (trough of EIA, red circle) appears at lower latitude, and another minimum (2nd minimum) appears over the epicenter.

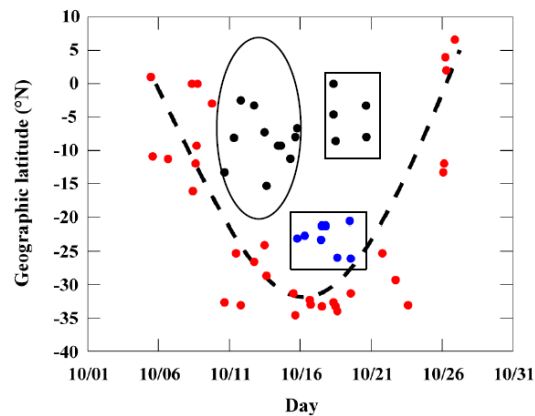


Fig.3 Geographical location of the 1, 2nd and 3rd minima of O⁺ density versus days day from 1 October to 31 st October. A minimum which first appears around equatorial region and another minimum which appears around the epicenter are marked by red circle. Black circle shows the 3rd minimum which appears between the two minimum.

As Fig.3 shows, the first minimum approaches to the second minimum as earthquake day is closer, that is EIA trough moves toward the epicenter position, and it finally merges into the epicenter on the earthquake day. During 11 October and 16 October, 3 minima appear. Black points surrounded by an black oval shows the 3rd minimum before the earthquake. Right after the earthquake, EIA related minimum (blue points surrounded by a black box) suddenly moves back toward the geomagnetic equator (being separated from the 2nd minimum colored by red circle). Between 17th- 20th October, 3rd minimum (black circle surrounded by black box) appears. The figure shows that the days of earthquake is a day when two minima merge.

Another 2 earthquakes occurred on the same day at nearly the same location on June 6 1981: First one at 06:5233, 16.467 N, and 98.293W, with M=6.9, and Depth of 8.3 km, and the second occurred at 10:59:39 at 16.519N, and 98.346 W with Ms of 6.9, and the depth of 18.2km. As two earthquakes occurred on the same days and nearly at the same place, the effect of these two earthquakes on the ionosphere can't be distinguished. Behavior of O⁺ along the satellite orbits which are within 60 ° from the epicenter is shown in Fig.4 during 2-9 days before. During the preparation phase of the earthquake, local time when the satellite flew over around the epicenter area is about 5-6 O'clock in the morning. This time period corresponds to the time when east ward natural electric field is weak or almost zero [Fejer et al., 1995]. The panel is arranged from the top for day of

earthquake, and to the bottom for 6 days 9, 8, 6, 5, 3, and 2 days before the earthquake. 10 days before the EQ, ionosphere is normal. The ionosphere starts to be modified from 9 days before the EQ. Two clefts of equatorial ionization anomaly is recognized 9 days before at 26°S and 10°N, with a small minimum at the epicenter latitude. This fact suggests that influence of earthquake is not so strong to change the general feature of EIA 9 days before. On the 8th before EQ (30 May 1982), in the satellite pass marked as 118.7° (about 20° west of the epicenter), one peak is identified over the epicenter. While for the satellite pass of 142.4° (34° to the west), one small peak appeared over the epicenter, and another larger peak at about 3°N appears. The former peak might be related to earthquake, while the latter one is related to EIA. 6 days before the EQ (1 Jun 1982), for a satellite pass of 88°W (about 8° east of the epicenter), at around 25°S, broad peak is identified. One more small peak can be seen 19S. The satellite pass of 111.8°W (20° west of the epicenter) shows one peak around 25°N, and the second peak at about 6°S (nearly 0° in geomagnetic latitude). 5 days before (2 June 1982), satellite pass of -84.5° (12°S east of the epicenter), the first peak is located over the epicenter, and the second peak is at 6° in geographic latitude, which is almost geomagnetic equator. For the satellite pass of 108°W (22° west of the epicenter), the first peak appears around at 23°, while the second peak appears at around 20°S. The former one might be related to the earthquake, while the latter is part of EIA. 4 days before (4 June 1982), the satellite pass of 77.4° shows a broad peak with a small minimum at around the epicenter. The second peak is identified around 25.30°S. The former might be related to the earthquake, while the latter is related to the EIA. 2 days before EQ, the satellite pass of 97.6°W (about 90.5° west of the epicenter) finds a peak over the epicenter latitude. For the satellite pass of 74.4°W, faint peak is over the epicenter marked by red arrow, and small peak over the geomagnetic equator marked by black arrow.

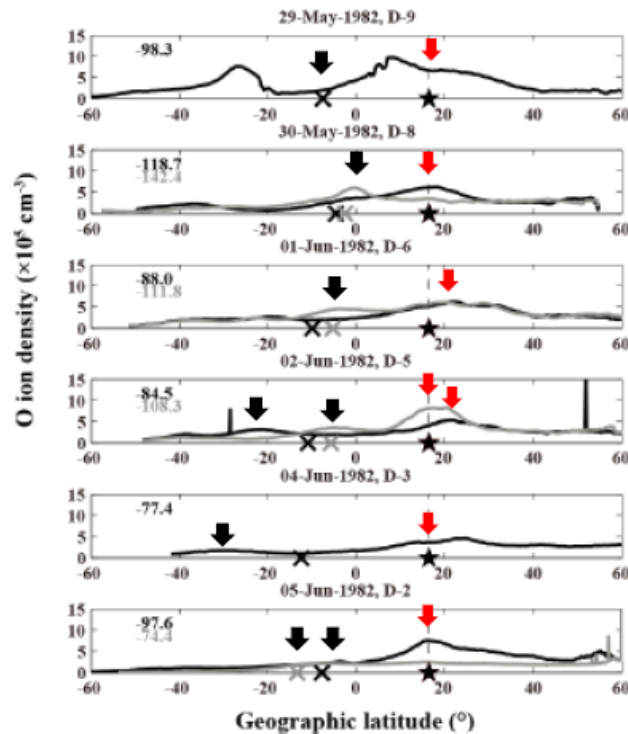


Fig.4 O⁺ density along satellite orbits which is within +/- 60° from the epicenter during 2-9 days before the earthquake. Colored numbers which are at the left side of each panel correspond to the satellite orbit of the same color. Red arrow shows the peak of O⁺ density, possibly related to earthquake. Black arrow shows EIA related peak.

3. Plasma drift observed by DE-2

We propose that ionosphere is modified by simply intensified dynamo electric field, and therefore we present here two supporting satellite orbits.

Fig.5 shows the part of the satellite orbits, 6 days before (10 Oct. 1981) for the earthquake which occurred on 16 Oct. 1981, $-33.1^{\circ}\text{N}/-73.1^{\circ}\text{E}$, $M_s=7.5$, $D=33\text{km}$. The location of the satellite at geographic equator crossing was 8.6°S , and 94.8°W at 15:45 UT. Therefore the satellite was 21.7° west from the epicenter longitude. Local time at geomagnetic equator crossing is 11:25 O'clock. Dashed vertical line with a star is drawn at the epicenter latitude, while dashed vertical line with a cross symbol shows the geomagnetic equator. In the upper panel, O^+ , M^+ , electron temperature T_e , and O^+ calculated from International Reference Ionosphere are shown in the disturbed region. In the lower panel, 3 components of plasma drift velocity are plotted together with satellite height. Although we are not sure of the reliability of absolute value of the plasma drift, the deviation from background velocity might be used for our discussion. A region between A and B or C and B is guessed as a region which is influenced by coming earthquake. From the molecular ion density measurement it increases suddenly at A, and reduces at B. On the other hand region C and B is the region where WE component is almost flat with respect to latitude. This is one of the features of disturbed region as we discuss later.

One component of plasma drift which is vertical to geomagnetic field changes its direction to upward from downward at around 52°S . Two stepwise increases of upward drift occur at A and C. So far we do not know whether we take a region between A and B, or we take the region C and B. We believe a stepwise increase between A and B is earthquake origin. The width of the disturbed region in latitude wise is about 30° if we take the region marked by A and B, 20° if we take the disturbed region as marked by C and B. The difference of the plasma drift between background plasma and that of disturbed region is about 5-10 m/sec. 2-4 mV/m. Although at the height of around 300 km, neutral wind still couples with ions, and this drift velocity might not be purely due to electric field, the plasma drift velocity should still provide some information on pure E field.

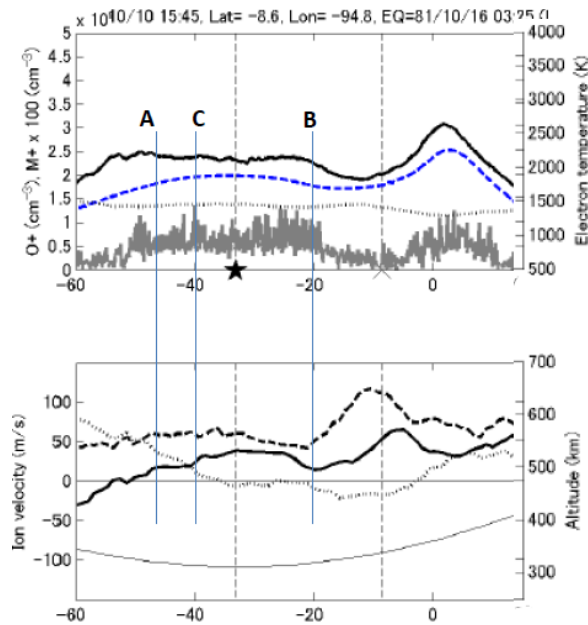


Fig. 5 6 days before the EQ 16 Oct. 1981, $-33.1^{\circ}\text{N}/-73.1^{\circ}\text{E}$, $M_s=7.5$, $D=33\text{km}$. The location of the satellite at geographic equator crossing was 8.6°S , and 94.8°W at 15:45 UT. The upper panel shows the O^+ density (thick black line), density of molecular ions (most probably NO^+ , gray line), electron temperature (dotted line) and O^+ calculated from IRI, dashed blue line) Vertical scale at the left is for O^+ density

8×10^6 electron /cc). 100 should be multiplied to the molecular ions. Scale at the right is for electron temperature. The lower panels shows east ward drift (eastward positive, dotted line), N/S component (toward North positive, dashed line), and upward drift (upward positive, thick black line) together with the satellite height. Dashed line with a star is marked as the epicenter latitude, while vertical dashed line with a cross symbol shows the geomagnetic equator. Lower panel shows plasma drift of three components, scaled at the left). Thin black line is a satellite height, which is scaled at the right. Vertical drift to geomagnetic line of force (thick black line: positive number shows upward direction), N-S component(dashed line, positive shows northward direction), and east-west component(dotted line, positive number shows eastward)

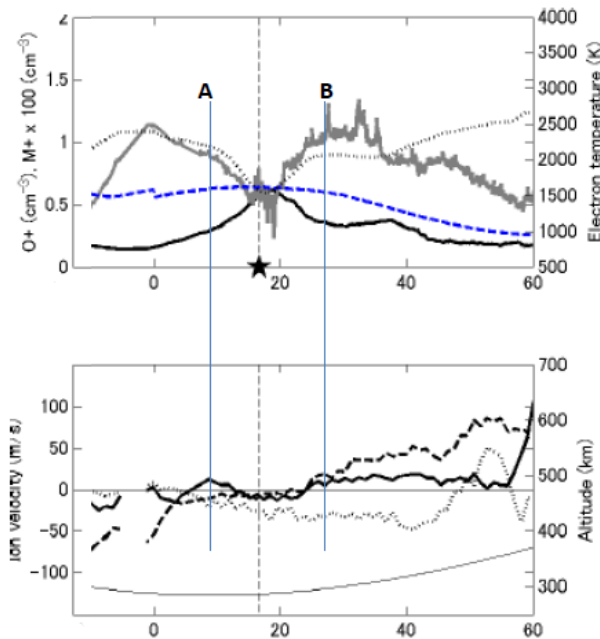


Fig.6 The same as for Fig.5 but 5 days before EQ which occurred on June 6 1982 (Fig.2). Satellite traversed geomagnetic equator (lat: 12.9° S, and 62° W) at 10:07UT, 1st June whose local time is about 6LT. The satellite was 36° east of the epicenter. A region marked A and B is considered to be a disturbed area As lower panel shows, at least from about 13° north to 25° in north, the plasma drift is downward. The width of drift reduced area is about 19° along latitude.

Fig.6 shows the same as of Fig.5 , but one satellite pass for 5 days before around the earthquake which occurred on 7 June 1982, 16.6° N, -96.15° E, $M_s=7$, $D=33.8$ km. Satellite traversed geographic equator located at Lat= 12.9° S, and long = 62.5° W at 10:07UT . Local time when the satellite crossed this longitude zone is therefore about 6 LT. Relation between O+ density and Te is antiphase. This might suggests that at the height of 300km , solar EUV already there.

The plasma drift is expected to be around zero according to Fejer and De Paula (1995) . At a region which is marked by A and B, upward plasma drift reduces with respect to the adjacent upward drift, and even negative. Suppose that plasma drift plotted here is accurate, antiphase variation of Te and Ne and reduced plasma drift in the disturbed area might be explained by some E field reducing mechanism. While, if real plasma drift value is negative than the positive(upward) which is measured, we can say that the west electric field is only enhanced in the disturbed region.

The difference of the vertical plasma drift between two earthquakes is; for the former, vertical drift increase, while it reduces for the latter case compared with the background plasma drift. This makes us guess that direction of E field for these two earthquakes are opposite in the disturbed region, which might depend on the local time of observation around the epicenter region as we discuss in the next section.

4 Discussion, Possible mechanism of ionosphere disturbance

The mechanism(s) of generating the ionosphere disturbances is most probably an electric field. However, generation mechanism of the electric field is not yet known.

Several mechanisms for the generation of the electric field and its effects on the ionosphere have been proposed. One is the stress-activated positive (or negative) hole [Freund et al., 2006]. Freund et al. claims that a large electric field is generated as a result of this mechanism. Several computer simulations were conducted with this idea [Kuo et al., 2014]. On the other hand, there is an argument that a current flowing into the ionosphere whose origin is in the ground might be too small to disturb the ionosphere [Pulinets and Ouzounov, 2010]. Pulinets and Davidenko [2014] suggest that radon emanation produces cluster ions, and then cloud formation occurs [Harrison et al., 2013], which finally produces latent heat. The cluster ions/aerosol size particles cause an air conductivity change and a humidity drop at a height close to the Earth's surface.

The ideas stated above suggest a change of single polarity in the ionosphere. On the other hand, satellite data analysis suggests a different mechanism for the ionosphere disturbance. According to our analysis of electron temperature, T_e , obtained with a Japanese satellite HINOTORI [Oyama et al., 2008] and O^+ with US satellite (DE-2) [Oyama et al., 2011]; the ionosphere behavior seems to be the same both west and east of the epicenter. The distribution of positive (negative) charges [Freund et al., 2006] suggests a reduced (increased) electric field in the west and an enhanced (reduced) electric field in the east. This might produce the asymmetry of the plasma behavior in the EW direction.

The variation of density of the atomic oxygen ion along the DE-2 satellite orbit which is shown in Fig.2 suggests that the electric field should have the same direction in the entire disturbed area. This leads us to propose a mechanism which is different from those proposed by Freund et al. [2006] and Pulinets and Davidenko [2014]. We propose that the usual eastward electric field during day and westward electric field at night in the ionosphere are simply enhanced. That is, during daytime, the eastward electric field is enhanced, and during night time westward E field is enhanced around the epicenter. It is noted, however that at this stage, we do not know how the day/night dynamo electric field is enhanced as we mention later.

Fig.7 illustrates schematically our idea of the enhancement of E field along E - W direction (E_x) in the disturbed region, E_x , both during daytime and night time respectively. We take EQ 16 Oct.1981, -33.1°N/-73.1°E, $M_s=7.5$, $D=33$ km. Both at the northern and southern edge of the disturbed area, direction of magnetic line of force is upward. Upper panel of Fig. 7 shows the direction of plasma drift during daytime and night time. During daytime plasma in the F region is lifted to higher altitude, and starts filling magnetic flux tube. During night time plasma is pushed down from higher to the lower altitude by westward electric field.

Suppose the potential which is generated by dynamo action between at both terminator edge of the globe is divided by Pedersen conductivity, the electric field distribution along EW direction can be expressed in the lower panel of Fig.7. In the lower panel, potential distributions for day and night are presented. During daytime, the potential is higher at the west of the globe with respect to the east edge of the globe. During night time the potential distribution reverses. The potential distribution which is shown in Fig.7 is one of two kinds of distribution. In Fig.8 two potential distributions are presented in the upper panel.

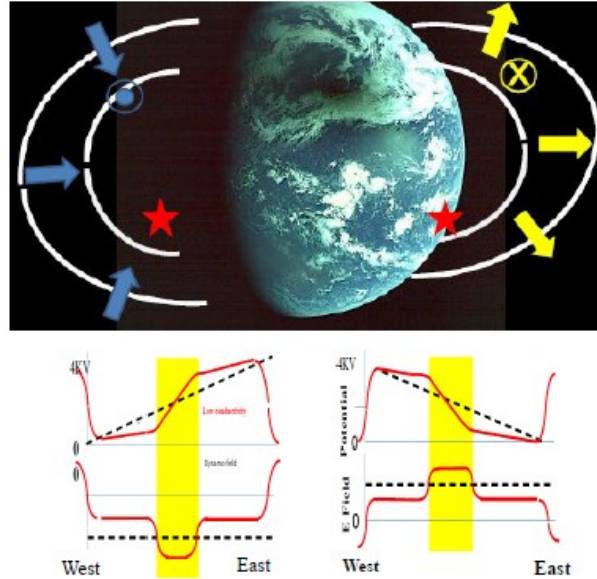


Fig.7 Schematic presentation on the direction of dynamo field (upper panel). Yellow and blue arrows show the upward and downward plasma drift during daytime and night time respectively. Lower panel shows one possible potential and E field distribution along the longitude. Left panel and right panel shows night time and daytime situation. Dashed black lines present potential and electric field when ionosphere is not influenced by earthquake both for day time and night time. Red lines shows potential distribution and electric field distribution reformed as a result of disturbance. More detail explanation is in the text.

First one is that enhanced potential drop in the disturbed area influences on other area as well whose potential distribution is presented by blue line. In this case enhanced potential drop in the disturbed area is higher/lower than the original distribution at west/east of non-disturbed area respectively. The disturbed area is marked by yellow box. The second distribution is that enhanced potential difference is limited to a disturbed area as shown by red line. No potential disturbance extends outside the disturbed area. Numbers 1, 2a, 2b, 3, 4a, 4b, and 5 above the potential distribution are placed for the convenience of further discussion. 1 and 5 is for outside of disturbed region. 2a and 4b are the inflexion points of the potential distribution of later case. 2b and 4b are the place of the maximum and minimum potential respectively. The regions 2a/2b and 4a/4b are transition from the non-disturbed to disturbed region. The second panel shows the Electric field distribution along EW direction. Electric field of former case is shown by blue line, and latter case by red line. It is noted that for the former distribution, electric field is reduced outside disturbed area (region 1 and 5). While for the latter case there is a region where electric field is lower than the ambient region at the both edges of the disturbed region (2a and 4b). The third panel shows roughly charge accumulation which is obtained by simply differentiation of the E field. For both electric field distributions shown in the second panel, plus charges and negative charge are generated at the east edge and west edge of the disturbed area. It might be noted here that these charges make the hole current flow in the dynamo region, and then changes the flow pattern of Sq current. This story suggests that Sq current system might be modified as a result of two Hall current system superposed to the original dynamo current system.

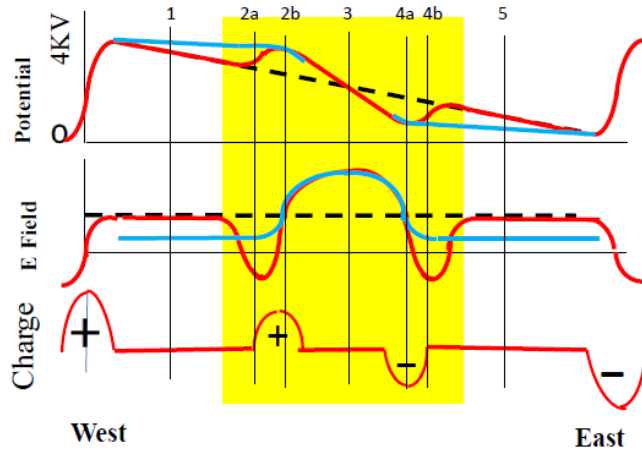


Fig.8 Schematic illustration of the potential and electric field around the disturbed area (yellow box) along west -east direction during daytime. The original potential and electric field distributions are drawn by a dashed black line in the upper panels, and by black dashed line in the middle panel respectively.

Based on Fig.8, we discuss the result observed with DE-2. The DE-2 satellite was a high inclination satellite, which crosses the disturbed area along North-South direction. Accordingly we present E_x along NS direction in Fig.9. The case in which potential is concentrated to the disturbed area (the latter case) is described. At the places 1 and 5, the electric field is the same as that of other non-disturbed area. At around 2a and 4b, the electric field is lower than the ambient. Depending on the degree of the disturbed area, the electric field might even be westward (which is the case shown in Fig.8). At point 2b and 4a, the electric field in the disturbed area is the same as that of non-disturbed area. The area between 2b and 4a is a region where the electric field is eastward.

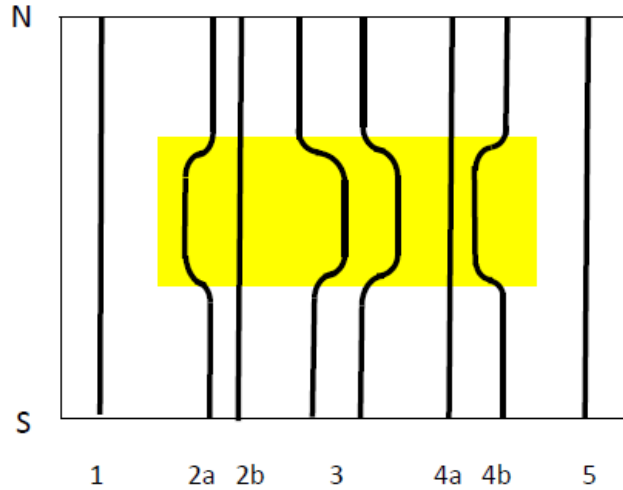


Fig.9 E_x distribution along North-South direction during daytime when eastward dynamo electric field is available. The distribution of the E field is for the case in which potential disturbance is concentrated to earthquake disturbing area. Number 1-5 correspond to the numbers in Fig. 8. Direction of the west/east ward electric field is negative/positive for the left /right direction respectively. It is noted that there might be regions where electric field is westward direction (2a, 4b) whole electric field is eastward direction.

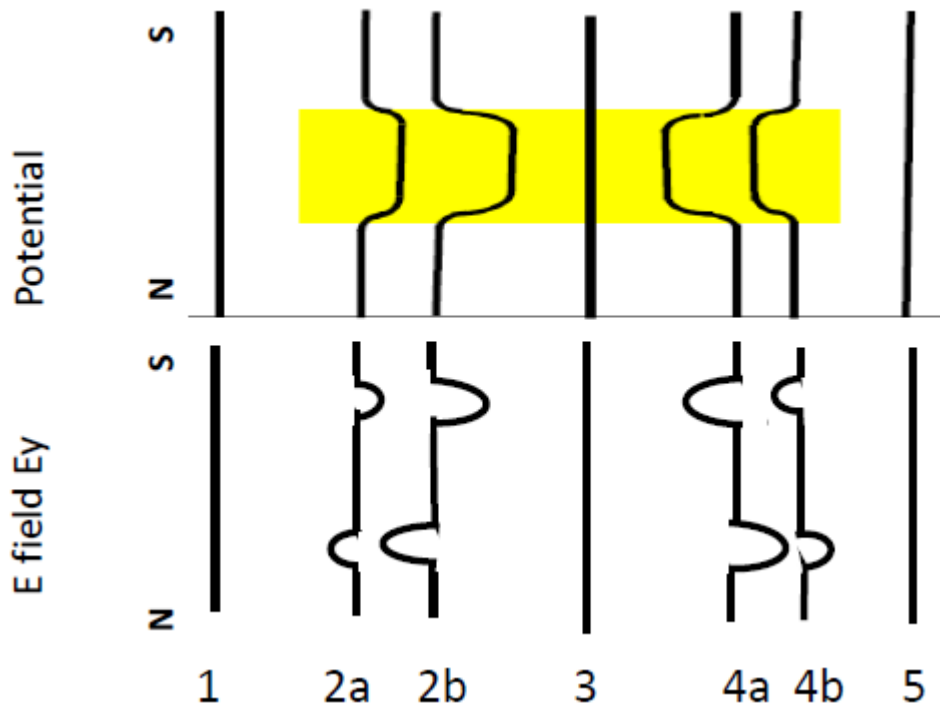


Fig.10 Potential (upper panel) and E field (E_y , lower panel) distribution along North-South direction. Yellow box is supposed to be disturbed area. The potential distribution is referred to the upper panel of Fig.8. Numbers 1-5 correspond to the locations marked in the upper panel of Fig.8. Outside the disturbed area, and over the epicenter (1, 3, 5), the potential is the same as those of non-disturbed area. Potential toward the right (left) direction is positive (negative) with respect to the non-disturbed region. By simply differentiating potential along NS direction, E field along NS direction, E_y , is schematically

shown in the lower panel.. From the potential distributions of at 2a and 2b , at the southern edge of disturbed zone the electric field is directed from disturbed area to non-disturbed area (southward direction). While at the northern edge, the electric field points from disturbed area to non-disturbed area(Northward direction)..

Potential and E field (E_y) distribution along N-S direction is schematically shown in Fig 10 for daytime. To draw this picture, potential distribution along EW direction which is shown in the upper panel of Fig.8 is used. Potential at non disturbed area of both west and east of the epicenter (1, and5) during earthquake preparation period is the same as that of the no -disturbed day. West of the epicenter, a region between 2a and 3 the potential is higher than the ambient. While at the east of the epicenter the potential in the disturbed area is lower than the ambient. Similar to the electric field along longitude, E_x , electric field along North-South direction, E_y , is obtained by simply differentiating the potential distribution along NS direction. If we assume that potential is the same in the whole disturbed area along NS direction, the electric field in the disturbed area is zero as shown in the lower panels of Fig.10. At the southern edge of the disturbed area at the west side of the epicenter, a positive charge appears, and electric field points toward south. Because of the southward direction of the E field, plasma drift toward west ward, while at the northern edge of the disturbed area, plasma drift points eastward. At the east edge of the disturbed area, the situation reverses. That is, the disturbed area is negative with respect to non-disturbed area. Accordingly the electric field at the southern edge point northward, while at the northern edge, electric field points southward.

When we compare Figure 5 with Fig.8, EW component, E_x in Fig. 8 well express the observed Electric field. That is, in the disturbed area, eastward E_x Field is enhanced. In Fig.5, in the region A-B, EW plasma drift which is caused by E_y shows almost zero. This behavior is consistent which is shown in the lower panels of Fig.10.

During night when electric field which points westward enhances as is the case shown in Fig.7. In summary behavior of plasma drift upward down ward plasma drift shown in Fig.5 and 6 can be explained by our idea.

5. Supporting evidences of AGW working

We mentioned that dynamo field is enhanced either due to reduced Pedersen conductivity around the height of 100KM or by change of wind system. Both will appear as results of the nonlinear/linear interaction of internal gravity wave and planetary scale wave.

The idea seems to be partly supported by Thermosphere Ionosphere Mesosphere Electrodynamics/Broad Band Emission Radiometry (TIMED/SABER) data. For the Pingtung and Wenchuan EQs, which occurred on May 8, 2008 (Depth = 19 km, $M_w = 7.9$) and on December 26, 2006 (Depth = 44 km, $M = 7.0$), respectively, NmF2 increases on the same day that the amplitude of the atmospheric temperature (T_n) variation of the 20–30 km wavelength range in vertical scale increases around the height of 100 km [Sun et al, 2011]. Fluctuations of VLF waves received as signals of transmitted radio waves have also been reported [Rozhnoi et al., 2007]. Muto et al. [2009] suggested the role of atmospheric gravity waves in the seismo-ionosphere perturbations as detected by sub-ionospheric VLF/LF propagation. These reports seem to suggest that atmospheric gravity waves (AGWs) propagated from near the Earth's surface break around the dynamo region. As a result, the breaking of these AGWs might produce the locally enhanced eastward electric field during day and the westward electric field during night. The role of AGWs has been discussed by Klimenko et al. [2011], who attributed the NmF2 increase to a change in the neutral composition. Very recently, the ionospheric response to infrasonic acoustic waves generated by natural hazard events has been reported [Zettergren and Snively, 2015]. Their computer simulations seem to support the idea that no clear disturbance appears directly above the epicenter. We expect that further study especially, computer simulation [Jin et al., 2012] should be

conducted on the role of gravity waves in the dynamo region. However, note that ionosphere disturbances may be caused by more than one mechanism.

5. Further tasks and need for a satellite constellation

We need to conduct further task. First of all we need to continue satellite data analysis. Data which can be used are Ne from CHAMP, and SWARM. There are other satellite such as DMSP and Formosat 1, which can provide us plasma drift and O+ density. As these two satellites are circular orbit, we can take a royal road for data analysis, that is, first construct a model, and then find the deviation from the model as we have done by using HINOTORI satellite data [Obama et al, 2008].

Secondly in order to identify the role of internal gravity wave, computer simulation on the effect of internal gravity wave need to be conducted. Klimenko et al [2011] assumed 10m/sec m and 600sec. of the amplitude, and period of internal gravity wave (IGW) at the height of 80 km. Their result shows clear ionosphere disturbance caused by IGW. Therefore next step for the computer simulation is to calculate the amplitude of IGW on the ground surface which is amplified to 10 m/sec at the height of 80 km. The computer simulation therefore should deal whole altitude from the ground surface, nonlinear interaction of the internal gravity wave and planetary scale wave.

Thirdly to identify global features of EQ precursors, satellite constellation mission is essential [Oyama et al., 2010]. Number of large EQ ($M > 7$) which occurs locally is small, which makes it difficult to identify common features. On the average one strong EQ ($M > 7$) occurs in Japan per year. Globally, about 10 strong EQs ($M > 7$) occur per year.

Further to identify the generation mechanism of E field, information of plasma density and electric field in a wide area such as 80° in longitude, and 40° in latitude is needed as we have shown in this manuscript. Ground-based observations, which are limited to a small geographic region such as Japan, are insufficient for a detailed assessment of the geographic extension of the affected area.

We need at least 6 satellites at nearly the same orbit altitude. Each satellite might be sun synchronous in order to observe the same location every two hours. Plasma probe which provide accurate and stable data [Oyama et al., 2015] should be accommodated. The accuracy of ionosonde and TEC data is insufficient to identify the epicenter, while satellite instruments can measure even small changes in plasma density.

6. Concluding remarks

To accelerate the study of ionosphere EQ precursors and confirm their applicability for predicting future EQs, a micro satellite constellation mission is essential. For the realization of such a mission, we need to identify definite persuasive signature from large EQs, which will make it possible to form a working group for the satellite mission.

While we prepare for such a near future satellite mission, further analysis of the existing data acquired from available satellites such as DMSP, CHAMP, FORMOSAT-3/COSMIC, and FORMOSAT-1 (ROCSAT-1) should be continued. We stress here that international collaboration can accelerate the process to get global morphology of ionosphere disturbance, as well as understand its physical mechanism.

Acknowledgements

We express our deep acknowledgement to the Mitsubishi Foundation for providing research Fund (ID: 26113). Our international collaboration was not possible without the support. Part of the research was supported by National Science Council of Taiwan (NSC101-211-M006-001, NSC101-219-M006-010) in 2013 and 2014. We also express our sincere thanks to Dr. Hui-Kuan Fang, of National Cheng Kung University, Tainan, Taiwan for plotting CHAMP satellite data. DE-2 data was analyzed by Dr. Y. Kakinami, Tomakomai Technical College, Hokkaido, Japan. We are thankful to all related agencies for providing us satellite (DMSP, DEMETER, CHAMP, and FORMOSAT-2/COSMIC) and ground based data (NmF2 and TEC).

References

- Astafyeva, E. and K. Heki, Vertical TEC over seismically active region during low solar activity, *J. Atmos. Solar Ter. Phys.*, 73, 1643-1652, 2011.
- Akhoondzadeh, M., M. Parrot, and M. R. Saradjian, Electron and ion density variations before strong earthquakes (M 6.0) using DEMETER and GPS data, *Nat. Hazards Earth Syst. Sci.*, 10, 7-18, 2010.
- Aleksandrin, S. Y., A. M. Galper, L. A. Grishantzeva, S. V. Koldashov, L. V. Maslennikov, A. M. Murashov, P. Picozza, V. Sgrigna, and S. A. Voronov, High energy particle bursts in the near-earth space as earthquake precursors, *Annales Geophys.*, 21, 597-602, 2003.
- Bankov, L. G., M. Parrot, R. A. Heelis, J. -J. Berthelier, P. G. Marinov, and A. K. Vassileva, DEMETER and DMSP satellite observation of the disturbed H^+/O^+ ratio caused by earth's seismic activity in the Sumatra area during December 2004, *J. Adv. Space Res.*, 46, 4, 419-430, 2010.
- Devi, M, A. K. Barbara, A. Depueva, Ya Yu, Ruzhin, and V. Depueva, Anomalous total electron content (TEC) and atmospheric refractivity prior to the very strong China earthquake of May 2008, *International Journal of Remote Sensing*, 31, No. 13, 3589-3599, 2010a.
- Devi, M., A. K. Barbara, P. Kashyap, A. Sepueva, Y. Y., Ruzhin, and V. Depueva, Earthquake time low latitude TEC and model estimated values: identification on earthquake induced atmospheric dynamics, *Adv. in Geosci.*, 26, 69-83, 2010b.
- Devi, M., A. Medhi, A. J. D. Sarma, and A. K. Barbara, Growth and Inhibition of Equatorial Anomaly Prior to an Earthquake (EQ): Case Studies with Total Electron Content (TEC) Data for Major EQs of Japan 2011 and Indonesia 2012, *Positioning*, 4, 240-252, 2013.
- Depueva, A., and N. M. Rotanova, Modification of low-latitude and equatorial ionosphere before large earthquakes, *Geomagn. Aero.* 40 (6), 50-54, 2000.
- Dobrovolsky, I. P., S. I. Zubkov, and V. I. Miyachkin, Estimation of the size of earthquake preparation zones, *Pure Appl. Geophys.*, 117, 1025-1044, 1979. doi: 1007/BF00876083.
- Fejer, B. G., and E. R. De Paula, Global equatorial ionospheric vertical plasma drifts measured by the AE-E satellite, *J. Geophys. Res.*, 100, 5769- 5776, 1995.
- Freund T. F., A. Takeuchi, and W. S. Lau, Electric currents streaming out of stressed igneous rocks—A step towards understanding pre-earthquake low frequency EM emissions, *Phys. Chem. Earth.*, 31, 389-396, 2006.
- Harrison, R. G., K. L. Aplin, and M. J. Rycroft, Earthquake- cloud coupling through the global atmospheric electric circuit, *Nat. Hazards Earth Syst., Sci.*, 1, 7271-7283, 2013.
- Hayakawa, M., Y. Kasahara, T. Nakamura, F. Muto, T. Horie, S. Maekawa, Y. Hobara, A. A. Rozhnoi, A. A., M. Solovieva, and O. A. Molchanov, A statistical study on the correlation between lower ionospheric perturbations as seen by subionospheric VLF/LF propagation and earthquakes, *J. Geophys. Res.*, 115, A09305, 2010.
- Jin, H., Y. Miyoshi, D. Pancheva, P. Mukhtarov, H. Fujiwara, and H. Shinagawa, Response of migrating tides to the stratosphere sudden warming in 2009 and their effects on the ionosphere studies by a whole

atmosphere- ionosphere model GAIA with F3/C and Timed/SABER observations, *J. Geophys. Res.*, 117, A10323, doi:10.1029/2012JA017650, 2012.

Jhuang, H. K., Y. Y. Ho, Y. Kakinami, J. Y. Liu, K. -I. Oyama, M. Parrot, K. Hattori, M. Nishihashi, and D. Zhang, Seismo-ionospheric anomalies observed by GPS-TEC before the 12 May 2008 M7.9 Wenchuan earthquake, *Inter. J. Remote Sensing*, 31 (13), 3579-3587T, 2010.

Karpov, I. V., and F.S. Bessarab, Model studying the effect of the solar terminator on the thermospheric parameters, *Geomag Aeronomy*, 48, 209- 219, 2008

Klimenko, M. V., V. V. Klimenko, I. V. Karpov, and I E. Zakharenkova, Simulation of Seismo-Ionospheric Effects initiated by internal gravity wave, *Russian J. Phys. Chemistry B*, 5, 393-401, 2011.

Kuo, C. L., L. C. Lee, and J. D. Huba, An improved coupling model for the lithosphere-atmosphere-ionosphere system, *J. Geophys. Res.*, 119, 3189-3205, 2014.

Liu, J. Y., Y. I. Chen, H. K. Jhuang, and Y. H. Lin, Ionospheric foF2 and TEC anomalous days associated with **M> 5.0 earthquake in Taiwan, during 1997 – 1999**, *Terr. Atmos. Oceanic Sci.*, 15, 371-383, 2004.

Liu, J. Y., Y. I. Chen, C. H. Chen, C. Y. Liu, C. Y. Chen, M. Nishihashi, J. Z. Liu, Y. Q. Xia, K. I. Oyama, and K. Hattori, and C. H. Lin, Seismo-ionospheric GPS TEC anomalies observed before the 12 May 2008 Mw7.9 Wenchuan Earthquake, *J. Geophys. Res.*, 114, A04320, 2009.

Oyama, K.- I., ,D. Minakshi , K. Ryu, C. H. Chen, J. Y. Liu H. Liu, L. Bankov and T. Kodama, Modification of ionosphere prior to large earthquakes- Report from Ionosphere precursor study group-, *Geosciences Lett*, 1-10, 3:6, DOI 10.1186/s40562^016-0038-3. 2016

Liu, J. Y., C. H. Chen, Y. I. Chen, W. H. Wan, K. I. Oyama, and K. W. Kuo, A statistical study of ionospheric earthquake precursors monitored by using equatorial ionization anomaly of GPS TEC in Taiwan during 2001-2007, *J. Asian Earth Sci.*, 39, 76-80, 2010.

Liu, J. Y., C. H. Chen, and H. F. Tsai, A statistical study on ionospheric precursors of the total electron content associated with 146 M > 6.0 earthquakes in Japan during 1998- 2011, *Earthquake Prediction Studies: Seismo Electromagnetics*, edited by Hayakawa, PP.1-13, TERRAPUB, 2014.

Liu, J., J. Huang, and X. Zhang, Ionospheric perturbations in plasma parameters before global strong earthquakes, *Adv. Space Res.*, 53, 776-787, 2014.

Muto, F. Y. Kasaha Mokhamad, N. G., and K. Heki, Ionospheric disturbances of the 2007 Bengkulu and the 2005 Nias earthquakes, Sumatra, observed with a regional GPS network, *J. Geophys. Res.*, 118, 1-11, 2013.

Muto, F. Y. Kasahara, Y. Hobara, M. Hayakawa, A. Rozhnoi, M. Solovieva, and O. A. Molchanov, Further study on the role of atmospheric gravity waves on the seismo-ionospheric perturbations as detected by subionospheric VLF/LF propagation, *Nat. Hazards Earth Sys. Sci.*,

9, 1111-1118, 2009.

Ouzounov, D., and F. Freund, Mid-infrared emission prior to strong earthquakes analyzed by remote sensing data, *Adv. Space Res.*, 33, 268-273, 2004.

Oyama, K. -I., Y. Kakinami, J. Y. Liu, M. Kamogawa, and T. Kodama, Reduction of electron temperature in low-latitude ionosphere at 600km before and after large earthquakes, *J. Geophys. Res.*, 113, A11317, 2008.

Oyama, K. -I., Y. Kakinami, J. Y. Liu, T. Kodama, and C. Y. Chen, Micro/mini satellites for earthquake studies - toward international collaboration, *Adv. in Geosci.*, 21, 251-256, 2010.

Oyama, K. -I., Y. Kakinami, J. Y. Liu, M. A. Abdu, and C. Z. Cheng, Anomalous Ion Density Latitudinal Distribution as a precursor of large earthquake, *J. Geophys. Res.*, 116, A04319, 2011.

Oyama, K.-I., C. H. Lee, H. K. Fang, and C. Z. Cheng, Means to remove electrode contamination effect of Langmuir probe measurement in space, *Rev. Sci. Instrum.* 83, 055113 (2012); <http://dx.doi.org/10.1063/1.4722167>.

Oyama K.-I., K. Ryu, C. H. Chen, D. Minakshi, H. Liu and J. Y. Liu, Diversity of ionosphere modification possibly caused by large earthquakes (ST09-A006), presented at AOGS, Aug.6 2015, 2015a.

Oyama K.-I., H. K. Fang, Y. Yakinami, K. Ryu, C. H. Chen, H. Liu, D. Minakshi and J. Y. Liu, Study on ionosphere precursor and International Reference Ionosphere, presented at IRI workshop, Thailand 9- 12, 2015, 2015b.

Oyama, K.-I., Y. W. Hsu, G. S. JIANG, W. H. Chen, H.K.Fang, C. Z. Cheng and W.T. Liu, Electron temperature and density probe for small aeronomy satellites, *Rev. Sci. Instr.* 86, 084703(2015), doi:10.1063/1.4927342, 2015.

Parrot, M., J. J. Berthelier, J. P. Lebreton, J. A. Sauvaud, O. Santolik, and J. Blecki, Examples of unusual ionospheric observations made by the DEMETER satellite over seismic regions, *Phys. Chem. Earth*, 31, 486-495, 2006.

Parrot, M., J. J. Berthelier, J. P. Lebreton, J. A. Sauvaud, O. Santolik, and J. Blecki, Ionospheric anomalies associated with the Haiti earthquake of 12 January 2010 observed by DEMETER satellite, *Nat. Hazards Earth Syst., Sci.*, 12, 671-678, 2012.

Pulinets, S., and D. Davidenko, Ionospheric precursors of earthquakes and Global circuit, *Adv. Space Res.*, 54, 709-723, 2014.

Pulinets, S., and D. Ouzounov, Lithosphere-Atmosphere- ionosphere coupling (LAIC) model-an unified concept for earthquake precursors validation, *J. Asian Earth. Sci.*, 41, 4-5, 371-382, 2010.

Rishbeth, H., Do Earthquake Precursors Really Exist? *Eos.*, 88 (29), 296-296, 2007.

Rodger, A. S., R. J. Mofett, and S. Qegan, The role of ion drift in the formation of ionization troughs in the mid- and high latitude ionosphere- a review, *J. Atmos. Terr. Phys.*, 54, 1-30, 1992.

Rozhnoi, A., M. Solovieva, O. Molchanov, P. -F. Biagi, and M. Hayakawa, Observation

evidences of atmospheric gravity waves induced by seismic activity from analysis of subionospheric LF signal spectra, 2007. *Nat. Hazard Earth Sci.*, 7, 625-628, 2007.

Ryu, K., E. Lee, M. Parrot, and K. -I. Oyama, Multisatellite observations of enhancement of equatorial ionization anomaly around Northern Sumatra earthquake of March 2005, *J. Geophys. Res.*, 119, 4767–4785, 2014a.

Ryu, K., E. Lee, J. S. Chae, M. Parrot, and S. Pulinets, Seismo-ionospheric coupling appearing as equatorial electron density enhancements observed via DEMETER electron density measurements, *J. Geophys. Res. Space Physics*, 119, 8524–8542, 2014b

Ryu, K., M. Parrot, S. G. Kim, K. S. Jeong, J. S. Chae, S. Pulinets, and K.-I. Oyama (2014), Suspected seismo-ionospheric coupling observed by satellite measurements and GPS TEC related to the M7.9 Wenchuan earthquake of 12 May 2008, *J. Geophys. Res. Space Physics*, 119, 10,305–10,323, 2014c

Ryu, K., K. -I. Oyama, L. Bankov, D. Minakshi, C.H. Koichi, J.Y. Liu, and H. Liu, Precursory Equatorial Ionospheric Density Enhancement: Contribution from Mid-latitude Large Earthquakes in the North-East Asian Region, *Adv. Space Res.*, 57, 268- 280, 2016

Saradjian, M. R., and M.Akhoondzadeh, Prediction of the date, magnitude and affected area impending strong earthquakes using integration of multiprecursors earthquake parameters, *Nat. Hazards Earth Syst. Sci.*, 11, 1109- 1119, 2011.

Sgrigna, V., L. Carota, L. Conti, M. Corsi, A. M. Galper, S. V. AKoldashov, A. M. Murashov, P. Picozza, R. Scrimaglio, and L. Stagni, Correlations between earthquakes and anomalous particle bursts from SAMPEX/PET satellite observations, *J. Atmos. Solar. Terr. Phys.*, 67, 1448-1462, 2006.

Sun, Y. Y., K. -I. Oyama, J. Y. Liu, H. K. Jhuang, and C. Z. Cheng, The Neutral Temperature in the Ionospheric Dynamo Region and the Relation with the Ionospheric Density during Wenchuan and Pingtung Earthquakes, *Nat. Hazard. Earth Syst. Sci.*, 11, 1759-1768, 2011

Wan, L. -W., X- H. Shen, Yu Zhang, and R. Yan, Preliminary proposal of scientific data verification in CSES mission, *Earthquake Sci.*, 28, 303-310, 2015.

Yigen, E., and M. Moldwin, The altitude extension of the mid-latitude trough and its correlation with plasma pause position, *Geophys. Res. Lett.*, 32, L09105, 2005.

Zakharenkova, I. E., I. I. Shagimuratov, A. Krankowski, and A. F., Lagovsky, Precursor phenomena observation in the electron content measurements before great Hokkaido earthquake of September 25, 2003,(M=8.3), *Stud. Geophyts. Geod.*, 51, 267-278, 2007.

Zhao, B., M. Wang, T. Yu, W. Wan, J. Lei, L. Liu, and B. Ning, Is an unusual large enhancement of ionospheric electron density linked with the 2008 great Wenchuan earthquake? *J. Geophys. Res.*, 113, A11304, 2008.

Zettergren, M. D., and J. B. Snively, Ionospheric response to infrasonic - acoustic waves generated by natural hazard events, *J. Geophys. Res.*, 40, 5345–5349, 2013.

Books

Ikeya, M., Earthquakes and Animals: “From folk legend to Science,” World Scientific, 2004.

Rikitake, T., Predictions and precursors of major earthquakes, Terra scientific publishing company, Tokyo, ISBN 4-88704-128-4, 2003.

Earthquake Prediction with Radio Techniques, Hayakawa, 2015
John Wiley & Sons, Singapore Pte. Ltd.
<http://onlinelibrary.wiley.com/book/10.1002/9781118770368>

Electrodynamic Coupling of Lithosphere–Atmosphere–Ionosphere of the Earth, Valery Sorokin, Vitaly Chmyrev, and Masashi Hayakawa, 2014
Nova Science Publishers
https://www.novapublishers.com/catalog/product_info.php?products_id=55228

Earthquake Prediction Studies: Seismo Electromagnetics, Edited by Masashi Hayakawa
Terra Scientific Publishing Company
<http://www.terrapub.co.jp/books/index.html>

The Frontier of Earthquake Prediction Studies, Ed. Hayakawa, 2012
Nihon Senmontosho Shuppan
<http://www.jpn-shuppan.co.jp/books/book8.html>

Ionospheric Precursors of Earthquakes, Sergey Pulinet and Kyrill Boyarchuk, 2004, Springer, <http://www.springer.com/us/book/9783540208396>